Supporting Information

Heteroatom Bay-Annulated Perylene Bisimides: New Materials for Organic Field Effect Transistors

Ravindra Kumar Gupta,[aΨ] Anamika Dey,[bΨ] Ashish Singh,[b] Parameswar Krishnan Iyer,*[a,b] and Achalkumar Ammathnadu Sudhakar*[a]

[a]*Department of Chemistry,*[b]*Centre for Nanotechnology*
Indian Institute of Technology Guwahati, Guwahati-781039, Assam. India.

E-mail: achalkumar@iitg.ac.in, pki@iitg.ac.in

[Ψ]Equal contribution

Table of Contents

1. Materials and methods

Commercially available chemicals were used without any purification; solvents were dried following the standard procedures. Chromatography was performed using either silica gel (60-120 mesh) or neutral aluminiun oxide. For thin layer chromatography, aluminium sheets pre-coated with silica gel were employed. IR spectra were recorded on a Perkin Elmer IR spectrometer at normal temperature by using KBr pellet. The spectral positions are given in wave number (cm^{-1}) unit. NMR spectra were recorded using Bruker 600 MHz NMR spectrometer. For ^{1}H NMR spectra, the chemical shifts are reported in ppm relative to TMS as an internal standard. Coupling constants are given in Hz. Mass spectra were determined from MALDI-TOF mass spectrometer using α-Cyano-4-hydroxycinnamic acid as a matrix or High Resolution Mass Spectrometer. Compounds were investigated for macroscopic structures (birefringence) by employing a polarizing optical microscope (Nikon Eclipse LV100POL) equipped with a programmable hot stage (Mettler Toledo FP90). Clean glass slides and coverslips were employed for the polarizing optical microscopic observations. The transition temperatures and associated enthalpy changes were determined by differential scanning calorimeter (Q20 DSC) under nitrogen atmosphere. The transition temperatures obtained from calorimetric measurements of the heating and cooling cycles at a rate of 5 °C/min are tabulated. Thermogravimetric analysis (TGA) was performed using thermogravimetric analyzer (Mettler Toledo, model TG/SDTA 851 e) under a nitrogen flow at a heating rate of 10 °C/min. UV-Vis spectra were obtained by using Perkin-Elmer Lambda 750, UV/VIS/NIR spectrometer. Fluorescence emission spectra in solution state as well as thin film state were recorded with Horiba Fluoromax-4 fluorescence spectrophotometer or Perkin Elmer LS 50B spectrometer. Fluorescence emission spectra in solution state and thin film state were recorded with Horiba Fluoromax-4 fluorescence spectrophotometer. Cyclic Voltammetry studies were performed using a Versa Stat 3 (Princeton Applied Research) Electrochemical workstation. DFT calculations were done on Gaussian 09 software package.

2. Experimental Section

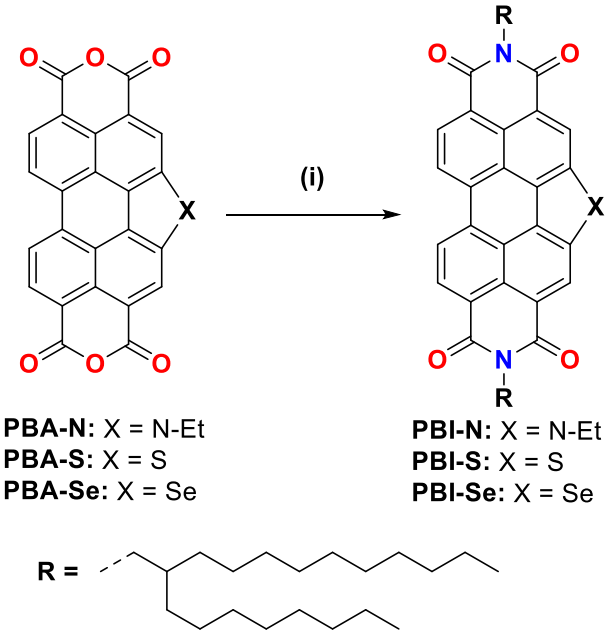

Scheme S1: Reagents and conditions. i) 2-octyldodecyl amine (**8**), imidazole, 160 ^{o}C, microwave, 30 min. (88-90%).

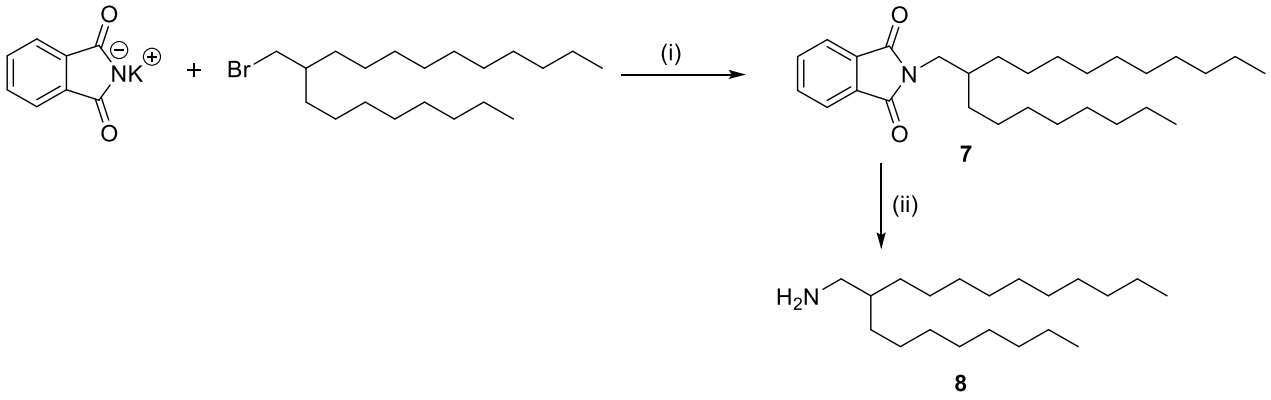

Scheme S2: Reagents and Conditions: i) dry DMF, 18 h, 90 ^{o}C, 95%; ii) $NH_2NH_2.H_2O$, methanol, 95 ^{o}C, 1 h, 95 %.

Synthesis of **4**, **5** and **6** were carried out according to previously reported procedures.[1]

Synthesis of 2-(2-octyldodecyl)isoindoline-1,3-dione (7)

Potassium phthalimide (23.53 mmol) was added to the solution of 2-octyldodecyl bromide (22.13 mmol) in DMF. The reaction mixture was stirred at 90 ^{o}C for 18 h. cooled the reaction mixture to room temperature, poured the mixture in water and extracted with methylene chloride several times. The combined organic layer was washed with 0.2 N KOH, water, saturated NH_4Cl, dried over anhy. Na_2SO_4 and concentrated under reduced pressure after filtration. The resulting crude compound was purified by column chromatography using methylene chloride as eluent.

7: R_f = 0.4 (10% EtoAc-Hexane); white solid, yield: 95%; IR (KBr pellet) ν_{max} in cm^{-1} 2921, 2851, 1773, 1714, 1593, 1503, 1467, 1435, 1391, 1343, 1326, 1247, 1234, 1119, 1095, 735; ^{1}H NMR (600 MHz, $CDCl_3$, 298 K): 7.85-7.82 (m, 2H, H_{Ar}), 7.72-7.70 (m, 2H, H_{Ar}), 3.57 (d, 2H, J = 7.3 Hz, N-CH_2), 1.88-1.86 (m, 1H, -CH), 1.28-1.23 (m, 32H, alkyl chain), 0.88-0.85 (m, 6H, -CH_3); ^{13}C NMR (150 MHz, $CDCl_3$, 298 K): δ 168.95, 134.02, 132.33, 123.36, 42.54, 37.22, 32.10, 31.68, 30.17, 29.84, 29.56, 26.50, 22.90, 22.88, 14.33; HRMS (ESI mode) exact mass calculated for $C_{28}H_{46}NO_2$ (M+1): 428.3523, found: 428.3519.

Synthesis of 2-octyldodecyl amine (8)

A mixture of compound **7** (16.4 mmol, 1 equiv.) and hydrazine hydrate (3 equiv.) in methanol were stirred at 95 ^{o}C for 1 h. after the disappearance of starting imide, methanol was removed under reduced pressure and residue was diluted with dichloromethane and washed with 10% KOH. The combined aqueous layer was extracted with dichloromethane. The combined organic layer was washed with brine and dried over $NaSO_4$. After removal of solvent the product obtained, which was used for next step without further purification.

8: R_f = 0.3 (20% EtoAc-Hexane); colorless liquid, yield: 95%; IR (KBr pellet) ν_{max} in cm^{-1} 3430, 2957, 2925, 2854, 1466, 1378, 720; ^{1}H NMR (600 MHz, $CDCl_3$, 298 K): 2.59 (d, 2H, J = 5.2 Hz, N-CH_2), 1.42, 1.30-1.26 (m, 35H, NH_2, alkyl chain), 0.88 (t, 6H, J = 6.8 Hz 2 × -CH_3); ^{13}C NMR (150 MHz, $CDCl_3$, 298 K): δ 45.45, 41.12, 32.14, 32.13, 31.76, 30.33, 29.90, 29.86, 29.57, 27.12, 27.01, 22.90, 14.34; HRMS (ESI mode) exact mass calculated for $C_{20}H_{44}N$ (M+1): 298.3468, found: 298.3466.

General procedure for synthesis of *bay*-annulated perylene bisimides (**PBI-N, PBI-S, PBI-Se**):

A mixture of *bay*-annulated perylene bisanhydrides **4**/**5**/**6** (0.18 mmol, 1 equiv.), 2-octyldodecyl amine (0.40 mmol, 2.2 equiv.) and imidazole (1 g) were taken in microwave vessel, flushed with nitrogen and put in microwave reactor. The mixture was heated to 160 ^{o}C for 30 minutes at 35 W. After cooling, reaction mixture was poured in 2N HCl (10 mL) and extracted with chloroform. Organic mixture was washed with water and saturated sodium chloride solution. The crude compound was purified by neutral alumina column chromatography using 50%

chloroform-hexane system further purification done by recrystallization from chloroform-methanol system.

PBI-N: R_f = 0.4 (20% EtoAc-Hexane); Dark red solid, yield: 88%; IR (KBr pellet) ν_{max} in cm^{-1} 2956, 2924, 2854, 1692, 1653, 1602, 1559, 1481, 1428, 1305, 1259, 804, 740; ^{1}H NMR (600 MHz, $CDCl_3$, 298 K): 8.98 (s, 2H, H_{Ar}), 8.92 (d, J = 7.98 Hz, 2H, H_{Ar}), 8.81 (d, J = 7.9 Hz, 2H, H_{Ar}), 4.97 (q, J = 7.4 Hz, 2H, N-CH_2), 4.26 (d, J = 7.3 Hz, 4H, N-CH_2), 2.07 (t, J = 6.4 Hz, 2H, -CH), 1.83 (t, J = 7.3 Hz, 3H, N-CH_2CH_3) 1.42-1.17 (m, 64H, alkyl chain), 0.83-0.80 (m, 12H, -CH_3); ^{13}C NMR (150 MHz, $CDCl_3$, 298 K): δ 165.42, 164.17, 134.26, 132.40, 127.57, 124.29, 123.65, 122.21, 121.62, 121.48, 119.28, 118.56, 45.17, 41.83, 37.08, 32.12, 32.11, 29.86, 29.85, 29.56, 29.55, 22.86, 16.98, 14.30; MALDI-TOF exact mass calculated for $C_{66}H_{94}N_3O_4$ (M+1): 992.7239, found: 992.198.

PBI-S: R_f = 0.4 (20% EtoAc-Hexane); Dark red solid, yield: 90%; IR (KBr pellet) ν_{max} in cm^{-1} 2956, 2924, 2853, 1693, 1654, 1596, 1432, 1311, 1246, 809, 743; ^{1}H NMR (600 MHz, $CDCl_3$, 298 K): 9.21 (s, 2H, H_{Ar}), 8.82 (s, 4H, H_{Ar}), 4.23 (d, J = 7.4 Hz, 4H, N-CH_2), 2.05 (t, J = 5.8 Hz, 2H, -CH), 1.25-1.18 (m, 64H, alkyl chain), 0.83-0.81 (m, 12H, -CH_3); ^{13}C NMR (150 MHz, $CDCl_3$, 298 K): δ 164.10, 163.67, 138.15, 132.71, 131.02, 129.47, 127.29, 125.78, 123.35, 122.74, 122.65, 122.33, 45.21, 32.13, 31.96, 30.35, 30.33,29.91, 29.89, 29.88, 29.85, 29.57, 26.78, 22.88, 14.32; MALDI-TOF exact mass calculated for $C_{64}H_{89}N_2O_4S$ (M+1): 981.6538, found: 981.086

PBI-Se: R_f = 0.4 (20% EtoAc-Hexane); Dark red solid, yield: 88%; IR (KBr pellet) ν_{max} in cm^{-1} 2955, 2924, 2853, 1694, 1652, 1593, 1558, 1431, 1349, 1309, 1245, 1165, 809, 743; ^{1}H NMR (600 MHz, $CDCl_3$, 298 K): 9.25 (s, 2H, H_{Ar}), 8.82 (s, 4H, H_{Ar}), 4.23 (d, J = 7.4 Hz, 4H, N-CH_2), 2.05 (t, J = 5.3 Hz, 2H, -CH), 1.25-1.18 (m, 64H, alkyl chain), 0.84-0.81 (m, 12H, -CH_3); ^{13}C NMR (150 MHz, $CDCl_3$, 298 K): δ 163.98, 163.65, 140.61, 133.83, 132.81, 129.61, 129.36, 125.99, 123.88, 122.83, 122.33, 121.89, 45.16, 32.13, 31.95, 30.36, 30.34, 29.92, 29.90, 29.88, 29.86, 29.58, 26.77, 22.89, 14.32; MALDI-TOF exact mass calculated for $C_{64}H_{89}N_2O_4Se$ (M+1): 1029.598, found: 1029.015.

3. NMR Spectra

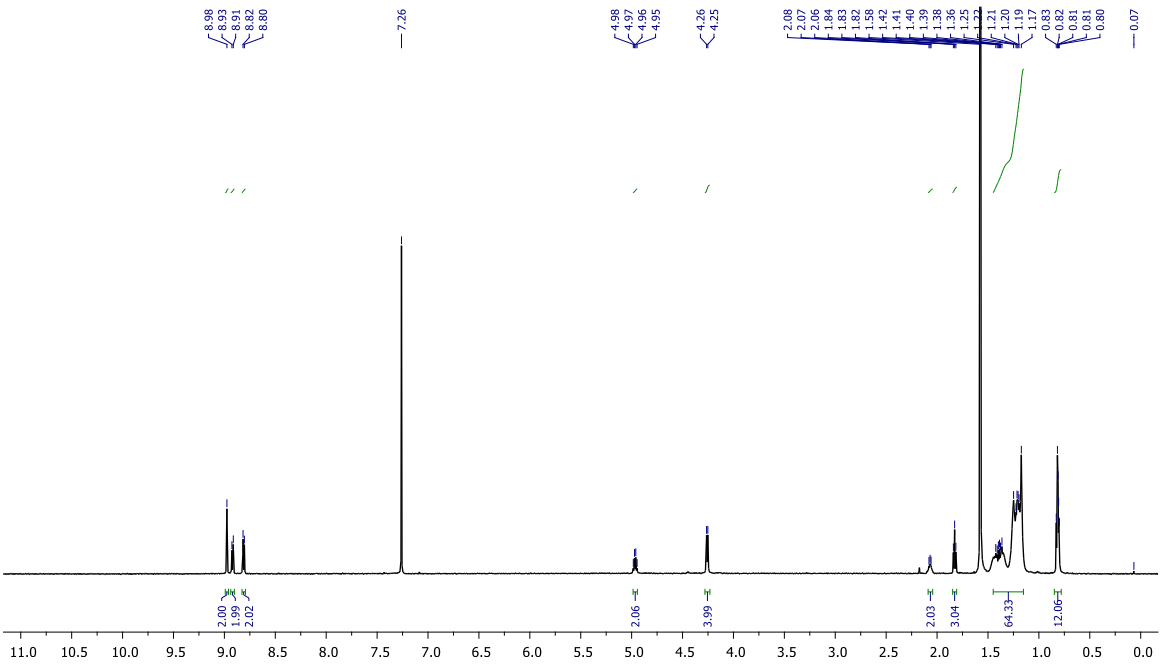

Figure S1. ^{1}H NMR (600 MHz) spectra of **PBI-N** in $CDCl_3$

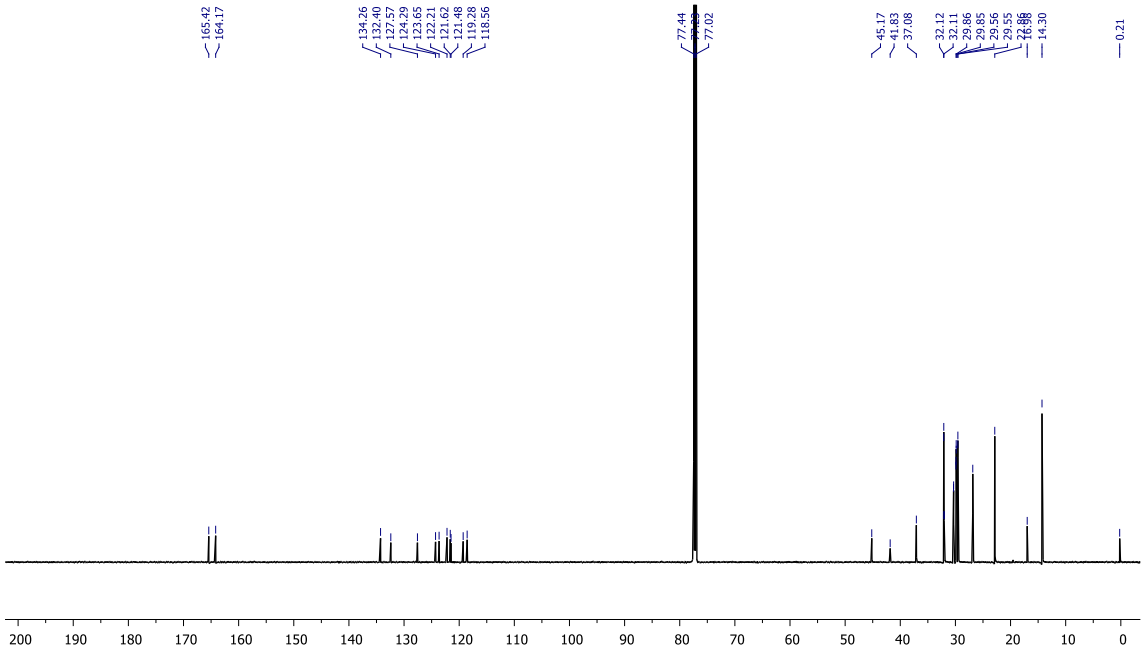

Figure S2. ^{13}C NMR (150 MHz) spectra of **PBI-N** in $CDCl_3$

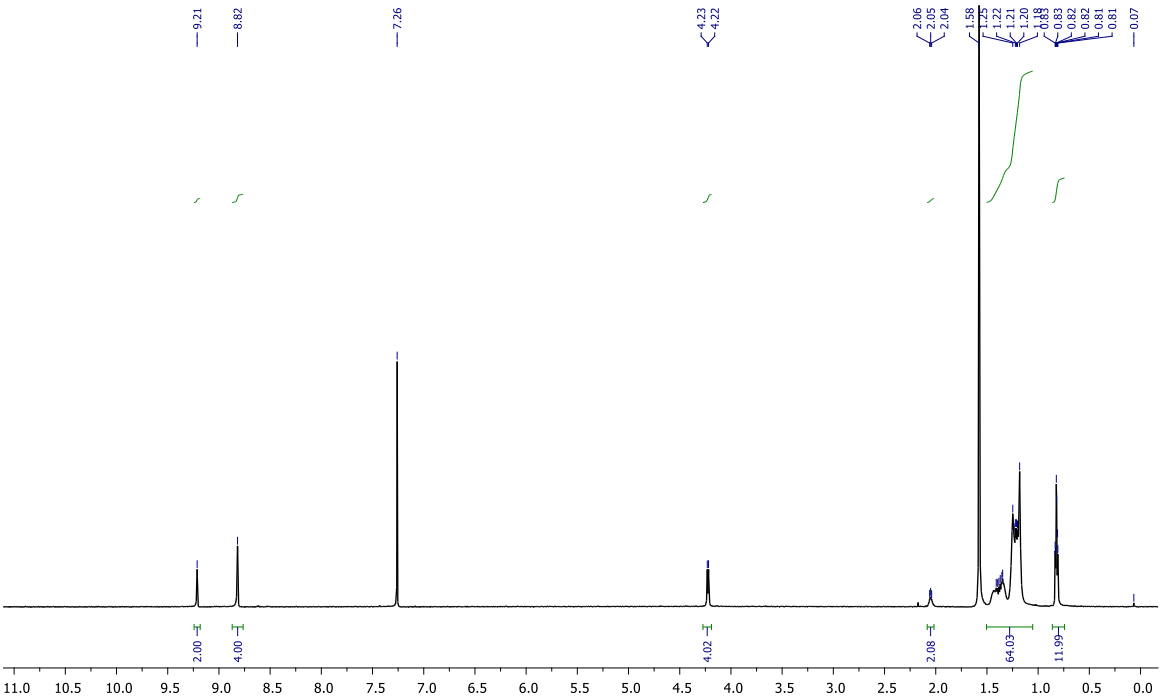

Figure S3. ^{1}H NMR (600 MHz) spectra of **PBI-S** in $CDCl_3$

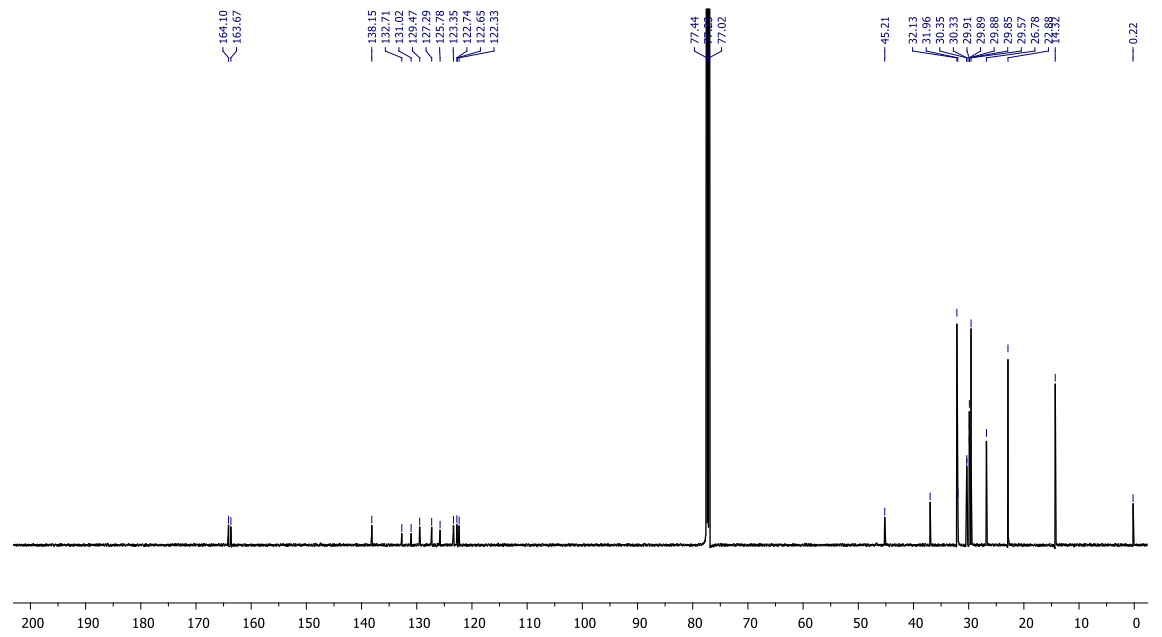

Figure S4. ^{13}C NMR (150 MHz) spectra of **PBI-S** in $CDCl_3$

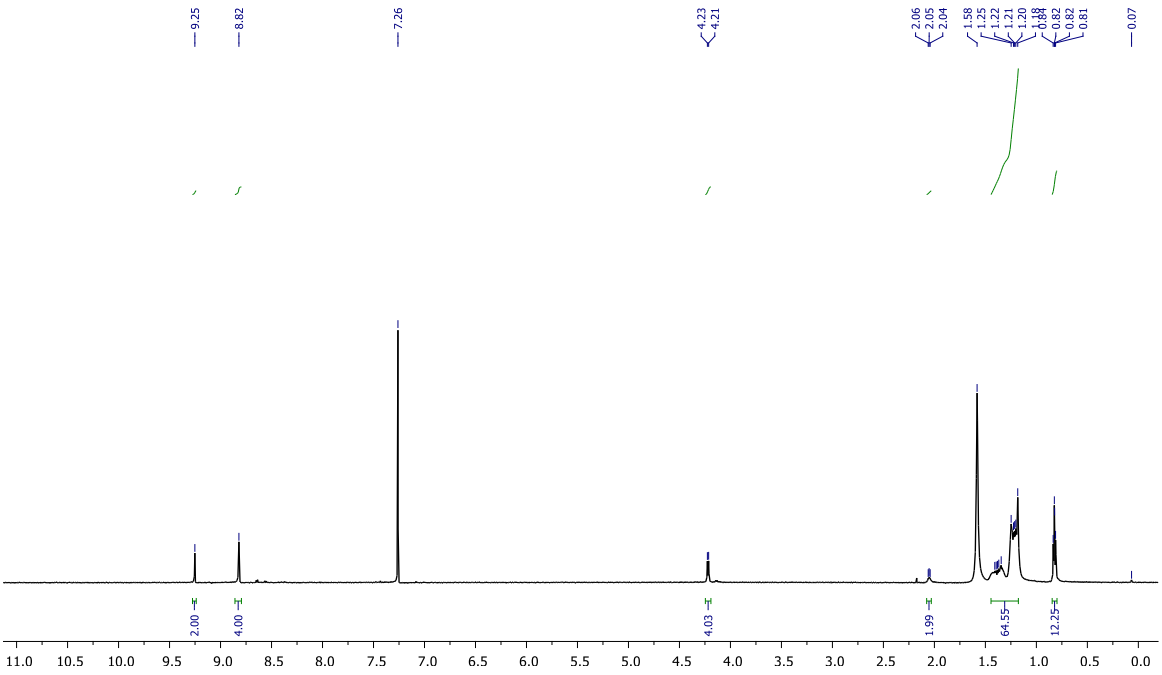

Figure S5. ^{1}H NMR (600 MHz) spectra of **PBI-Se** in $CDCl_3$

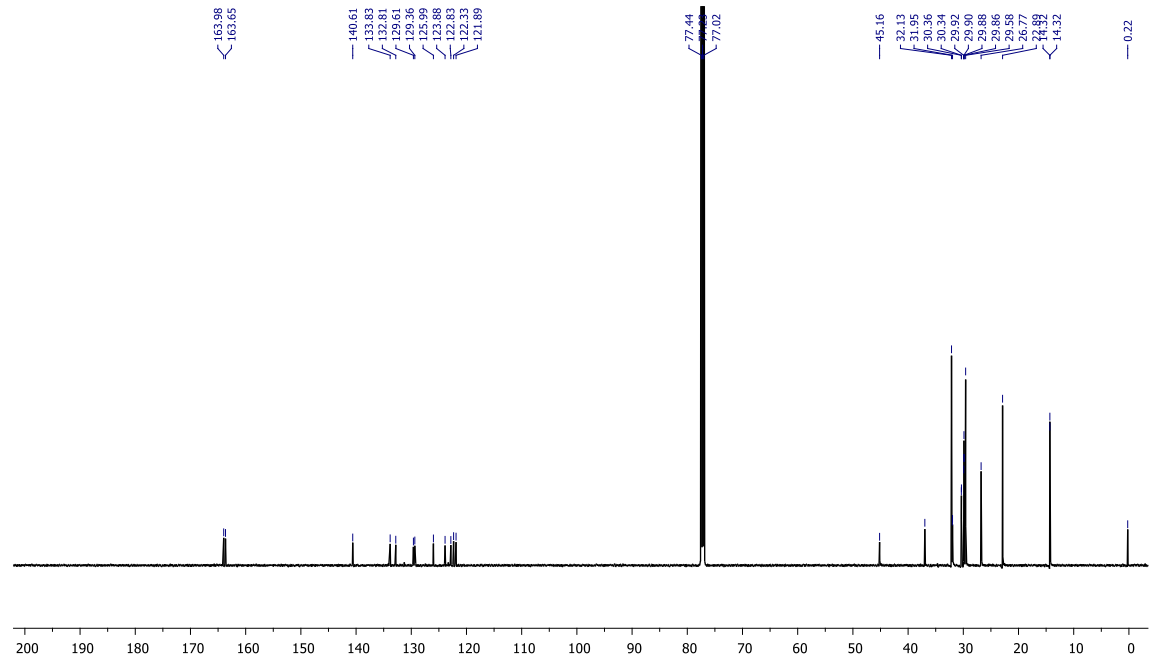

Figure S6. ^{13}C NMR (150 MHz) spectra of **PBI-Se** in $CDCl_3$

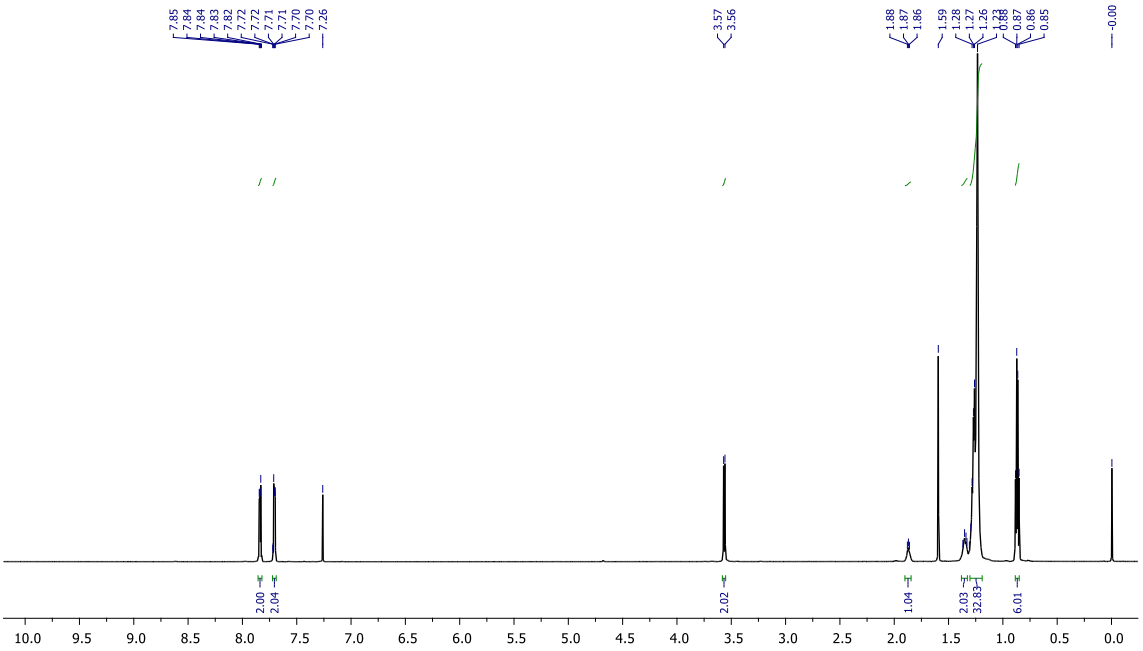

Figure S7. ^{1}H NMR (600 MHz) spectra of **7** in $CDCl_3$

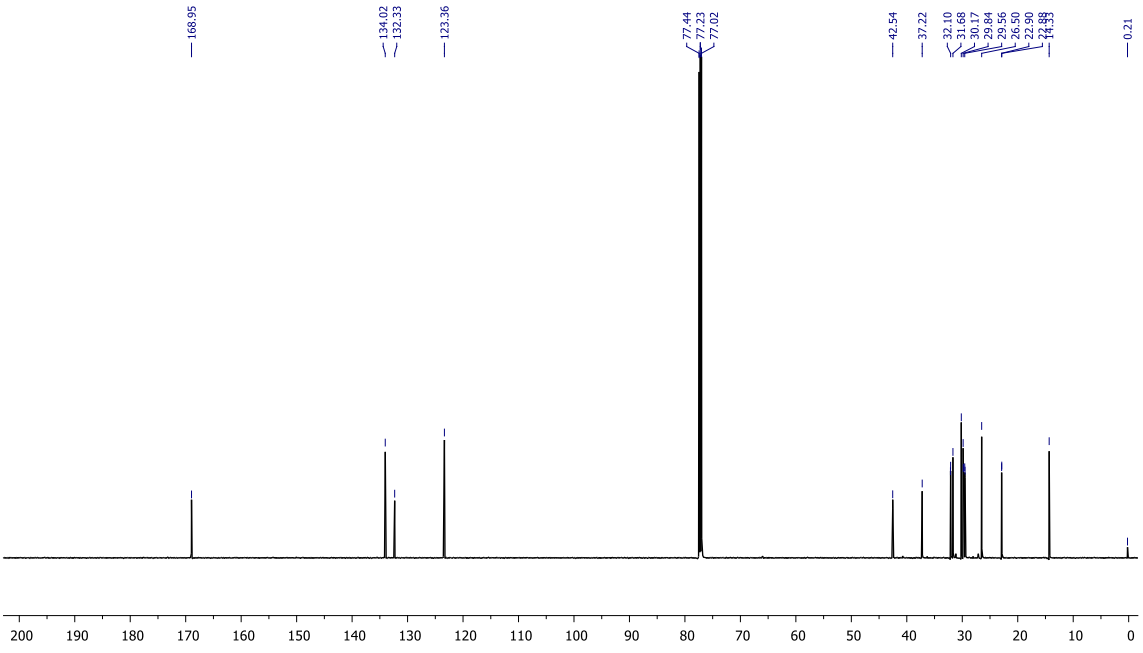

Figure S8. ^{13}C NMR (150 MHz) spectra of **7** in $CDCl_3$

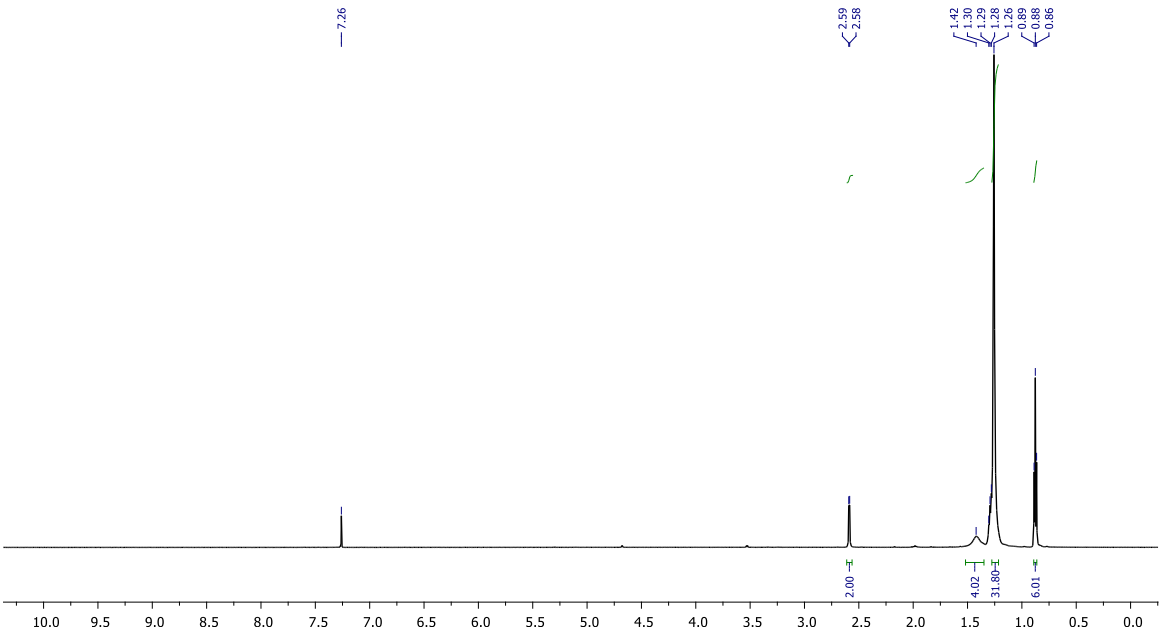

Figure S9. ^{1}H NMR (600 MHz) spectra of **8** in $CDCl_3$

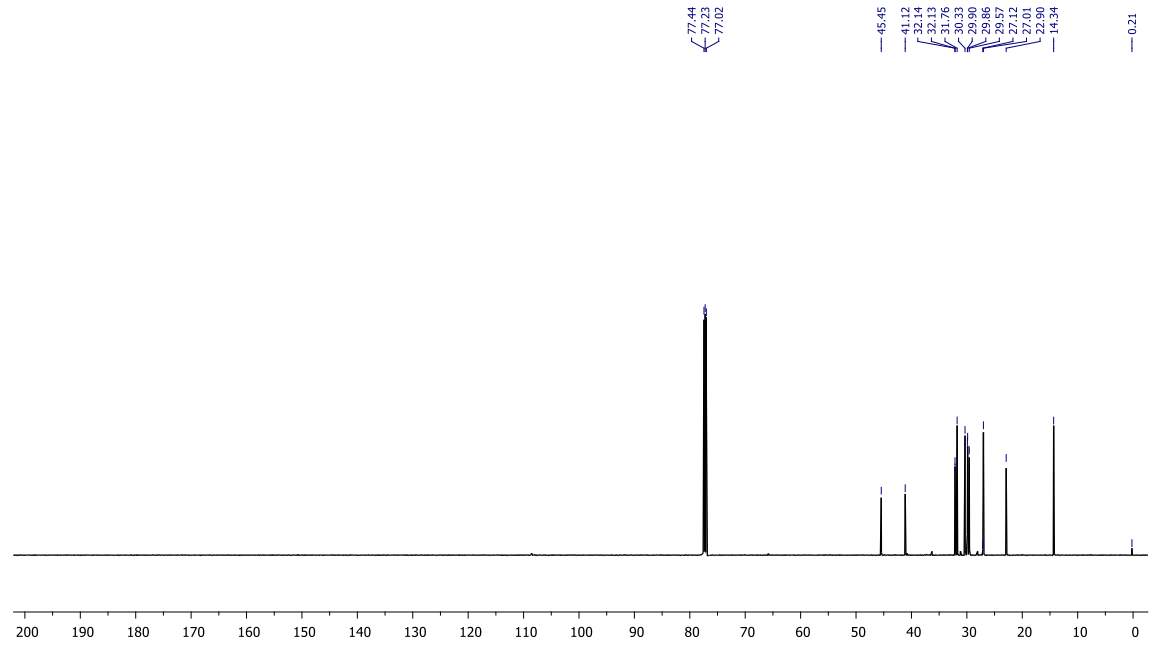

Figure S10. ^{13}C NMR (150 MHz) spectra of **8** in $CDCl_3$

4. MALDI-TOF mass spectra

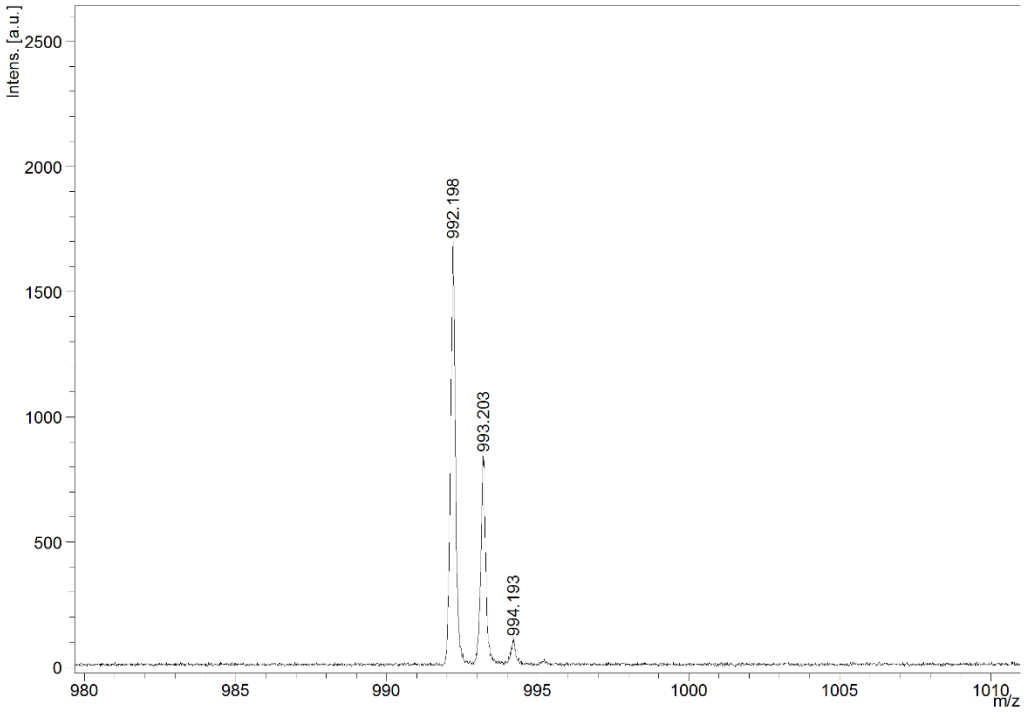

Figure S11. MALDI-TOF mass spectrum of **PBI-N.**

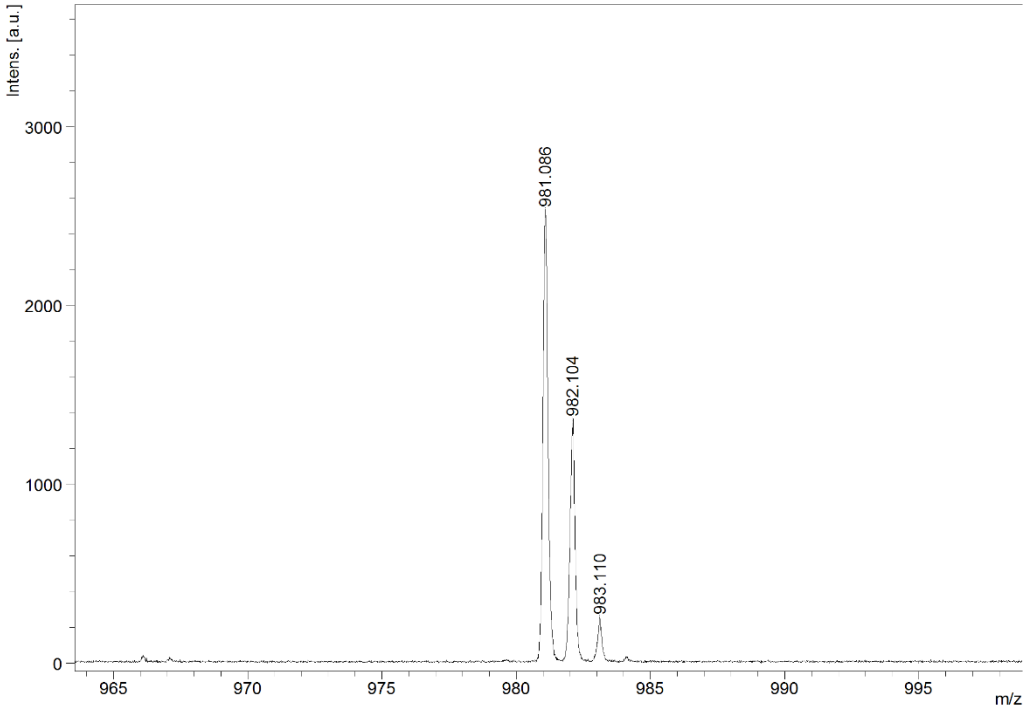

Figure S12. MALDI-TOF mass spectrum of **PBI-S.**

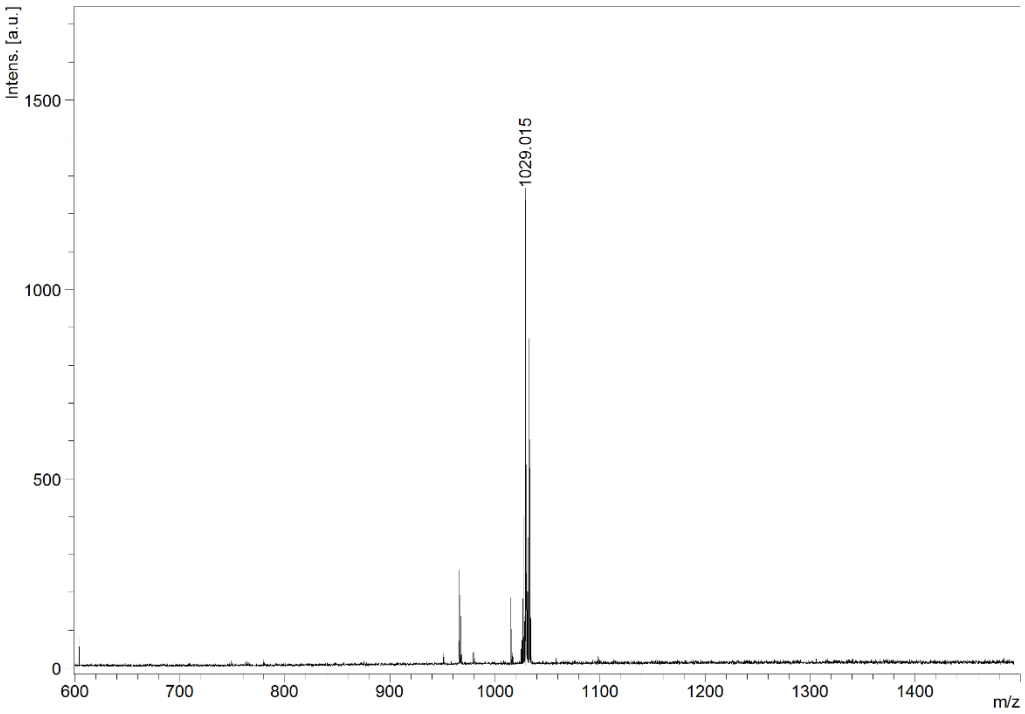

Figure S13. MALDI-TOF mass spectrum of **PBI-Se.**

5. Thermogravimetric analyses (TGA)

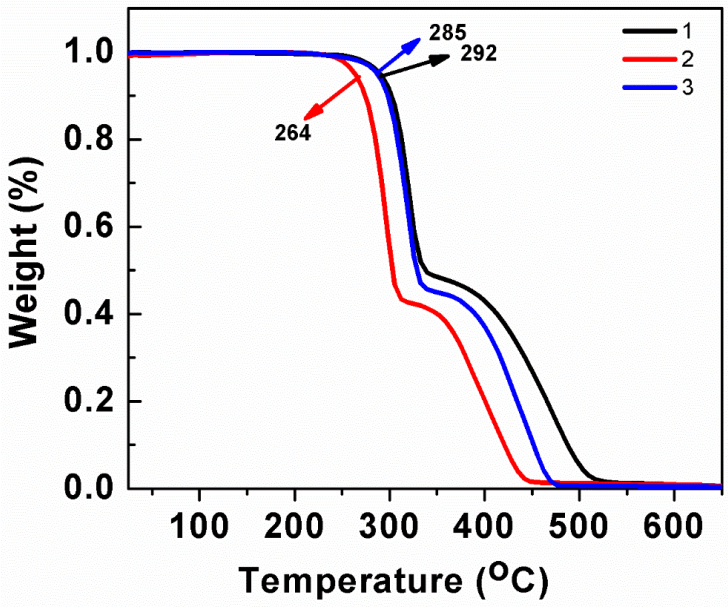

Figure S14. TGA curve obtained for compounds at a rate of 10 ^{o}C/min under N_2 atmosphere (**1: PBI-N; 2: PBI-S; 3: PBI-Se**)

6. Computational studies

To understand the electronic properties and frontier molecular orbital energy level of compound **PBI-N** was done at B3LYP/6-31g(dp) method using Gaussian 09 program package.[2] The absence of imaginary frequency ensured the energy minimized structure of all the compounds.

Table S1: Molecular orbital energies and diagrams of compound **PBI-N.**

PBI-N	Orbital Energy	Orbital Diagram
LUMO + 1	-1.75 eV	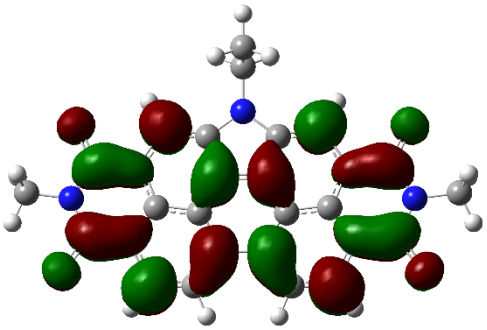
LUMO	-3.19 eV	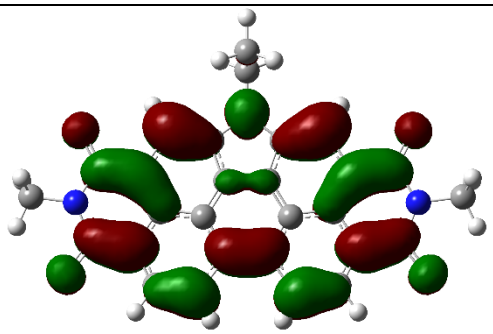
HOMO	-5.87 eV	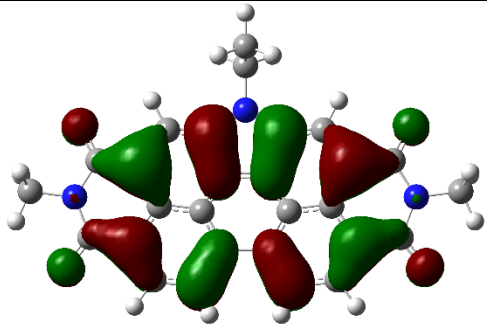

HOMO -1	-6.47 eV	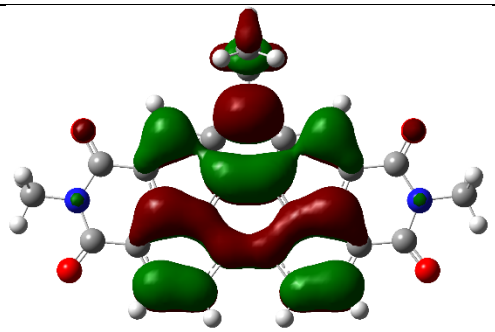

DFT calculation data for PBI-N

Standard orientation:

Center Number	Atomic Number	Atomic Type	Coordinates (Angstroms) X	Y	Z
1	6	0	2.992426	-2.911678	0.126094
2	6	0	1.592439	-3.056564	0.145442
3	6	0	0.745661	-1.939455	0.086415
4	6	0	1.422107	-0.678927	0.010654
5	6	0	2.819757	-0.507174	-0.014895
6	6	0	3.617263	-1.662647	0.045615
7	6	0	0.687585	0.492496	-0.051674
8	6	0	1.146360	1.804788	-0.148247
9	6	0	2.551496	1.975525	-0.173549
10	6	0	3.349715	0.824559	-0.105925
11	6	0	-0.745650	-1.939455	0.086449
12	6	0	-1.422098	-0.678927	0.010726
13	6	0	-0.687579	0.492496	-0.051642
14	6	0	-1.592425	-3.056565	0.145495
15	6	0	-2.992413	-2.911679	0.126211
16	6	0	-3.617253	-1.662645	0.045798
17	6	0	-2.819750	-0.507173	-0.014750
18	6	0	-3.349712	0.824560	-0.105762
19	6	0	-2.551496	1.975523	-0.173456
20	6	0	-1.146359	1.804787	-0.148207
21	6	0	4.824374	0.970158	-0.130846
22	7	0	5.587825	-0.212446	-0.067368
23	6	0	5.090764	-1.531098	0.020323
24	6	0	-5.090756	-1.531093	0.020623
25	7	0	-5.587817	-0.212461	-0.067377
26	6	0	-4.824373	0.970162	-0.130592
27	8	0	5.387733	2.055399	-0.202847
28	8	0	5.843928	-2.493765	0.071360
29	8	0	-5.843914	-2.493783	0.071296
30	8	0	-5.387729	2.055378	-0.202970
31	7	0	-0.000001	2.625258	-0.215843

32	6	0	-0.000006	4.086243	-0.242480
33	6	0	-0.000087	4.717507	1.152078
34	6	0	7.043833	-0.027072	-0.095903
35	6	0	-7.043821	-0.027117	-0.096272
36	1	0	3.626623	-3.790692	0.171976
37	1	0	1.179035	-4.058578	0.205606
38	1	0	3.052512	2.935211	-0.242545
39	1	0	-1.179018	-4.058579	0.205630
40	1	0	-3.626607	-3.790692	0.172126
41	1	0	-3.052514	2.935211	-0.242425
42	1	0	0.878245	4.405731	-0.811821
43	1	0	-0.878191	4.405729	-0.811924
44	1	0	-0.000093	5.808673	1.069408
45	1	0	-0.886344	4.417088	1.718216
46	1	0	0.886113	4.417103	1.718312
47	1	0	7.356185	0.587029	0.751287
48	1	0	7.504030	-1.010388	-0.046115
49	1	0	7.333545	0.487598	-1.014271
50	1	0	-7.503995	-1.010517	-0.047959
51	1	0	-7.356627	0.585798	0.751626
52	1	0	-7.333108	0.488802	-1.014058

Total Energy (HF) = 3480.6865026625 Hartrees

Table S2: Molecular orbital energies and diagrams of compound **PBI-S.**

PBI-S	Orbital Energy	Orbital Diagram
LUMO + 1	-1.95 eV	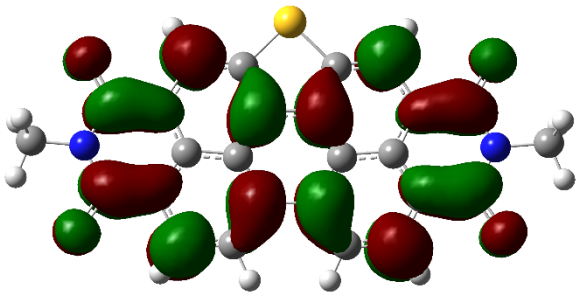
LUMO	-3.44 eV	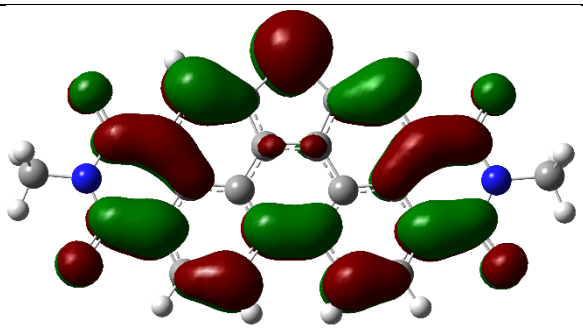

HOMO	-6.15 eV	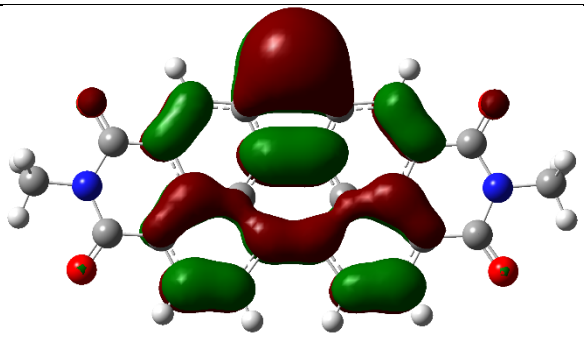
HOMO -1	-6.86 eV	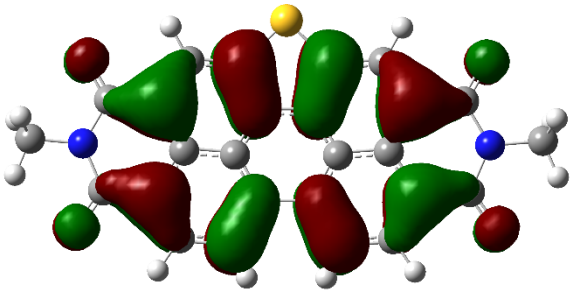

DFT calculation data for PBI-S.

Standard orientation:

Center Number	Atomic Number	Atomic Type	Coordinates (Angstroms) X	Y	Z
1	6	0	2.948740	-2.692644	0.000009
2	6	0	1.548317	-2.787592	0.000005
3	6	0	0.740694	-1.643745	0.000034
4	6	0	1.425036	-0.386985	0.000057
5	6	0	2.834459	-0.278207	0.000086
6	6	0	3.599868	-1.460257	0.000073
7	6	0	0.700968	0.814039	0.000046
8	6	0	1.276797	2.083784	0.000055
9	6	0	2.682915	2.189681	0.000060
10	6	0	3.436175	1.018611	0.000099
11	6	0	-0.740695	-1.643744	0.000024
12	6	0	-1.425035	-0.386983	0.000013
13	6	0	-0.700965	0.814040	0.000024
14	6	0	-1.548321	-2.787589	0.000024
15	6	0	-2.948744	-2.692640	0.000000
16	6	0	-3.599870	-1.460252	-0.000048
17	6	0	-2.834457	-0.278205	-0.000008
18	6	0	-3.436170	1.018615	0.000045
19	6	0	-2.682909	2.189684	0.000060
20	6	0	-1.276791	2.083785	0.000028
21	6	0	4.917032	1.114547	0.000102

22	7	0	5.635756	-0.093020	0.000200
23	6	0	5.079652	-1.387018	0.000092
24	6	0	-5.079657	-1.387006	-0.000184
25	7	0	-5.635754	-0.093013	-0.000399
26	6	0	-4.917027	1.114556	0.000279
27	8	0	5.512865	2.183257	-0.000310
28	8	0	5.786763	-2.384959	-0.000294
29	8	0	-5.786802	-2.384922	0.000196
30	8	0	-5.512847	2.183274	0.000260
31	16	0	0.000004	3.321890	0.000062
32	6	0	7.098389	0.034116	0.000041
33	6	0	-7.098388	0.034088	-0.000523
34	1	0	3.557728	-3.590199	-0.000020
35	1	0	1.099068	-3.775039	-0.000028
36	1	0	3.206525	3.139386	0.000054
37	1	0	-1.099074	-3.775037	0.000029
38	1	0	-3.557734	-3.590193	-0.000020
39	1	0	-3.206517	3.139390	0.000152
40	1	0	7.421096	0.588721	0.883363
41	1	0	7.518090	-0.968318	0.002158
42	1	0	7.421469	0.584864	-0.885602
43	1	0	-7.518055	-0.968354	-0.005409
44	1	0	-7.421983	0.582431	0.886448
45	1	0	-7.420614	0.591064	-0.882501

Total Energy (HF) = 3281.7667429928 Hartrees

Table S3: Molecular orbital energies and diagrams of compound **PBI-Se.**

PBI-Se	Orbital Energy	Orbital Diagram
LUMO + 1	-1.93 eV	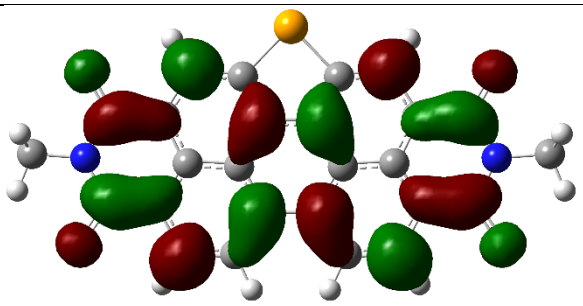

LUMO	-3.42 eV	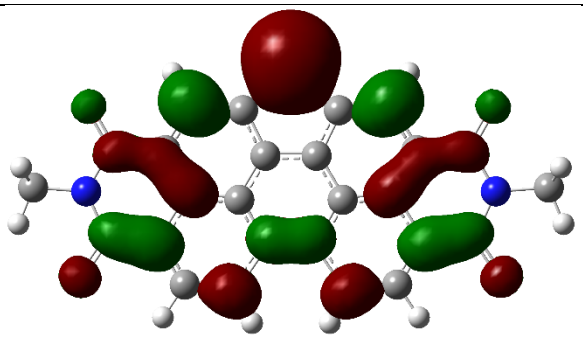
HOMO	-6.12 eV	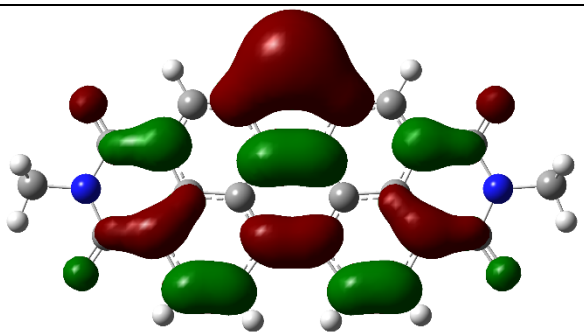
HOMO -1	-6.68 eV	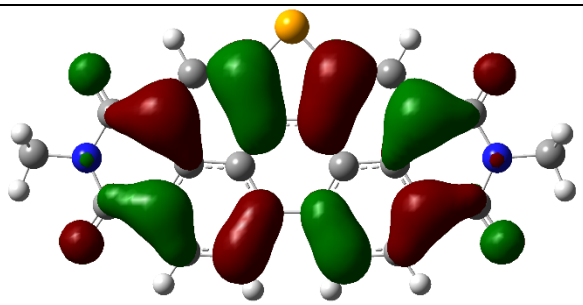

DFT calculation data for PBI-Se

Standard orientation:

Center Number	Atomic Number	Atomic Type	Coordinates (Angstroms) X	Y	Z
1	6	0	-2.933083	-2.945428	0.000004
2	6	0	-1.533452	-3.022169	-0.000009
3	6	0	-0.738656	-1.869795	-0.000001
4	6	0	-1.424771	-0.614375	0.000026
5	6	0	-2.838582	-0.529368	0.000059
6	6	0	-3.593113	-1.719286	0.000042
7	6	0	-0.705798	0.596320	0.000019
8	6	0	-1.320878	1.849996	0.000039

9	6	0	-2.725219	1.930172	0.000070
10	6	0	-3.464248	0.753565	0.000096
11	6	0	0.738656	-1.869795	-0.000025
12	6	0	1.424771	-0.614375	-0.000033
13	6	0	0.705799	0.596320	-0.000010
14	6	0	1.533452	-3.022169	-0.000036
15	6	0	2.933083	-2.945428	-0.000054
16	6	0	3.593113	-1.719286	-0.000074
17	6	0	2.838583	-0.529368	-0.000061
18	6	0	3.464249	0.753565	-0.000066
19	6	0	2.725220	1.930172	-0.000027
20	6	0	1.320879	1.849996	-0.000007
21	6	0	-4.945608	0.833075	0.000183
22	7	0	-5.649773	-0.381450	0.000084
23	6	0	-5.073950	-1.666014	0.000023
24	6	0	5.073950	-1.666015	-0.000092
25	7	0	5.649773	-0.381451	-0.000101
26	6	0	4.945608	0.833074	-0.000106
27	8	0	-5.553222	1.895422	-0.000066
28	8	0	-5.766273	-2.674576	-0.000077
29	8	0	5.766269	-2.674579	0.000042
30	8	0	5.553222	1.895421	0.000093
31	34	0	0.000000	3.216529	0.000020
32	6	0	-7.113895	-0.274034	-0.000004
33	6	0	7.113895	-0.274032	-0.000019
34	1	0	-3.532764	-3.849188	-0.000016
35	1	0	-1.072450	-4.004001	-0.000036
36	1	0	-3.261288	2.872920	0.000098
37	1	0	1.072450	-4.004001	-0.000028
38	1	0	3.532764	-3.849188	-0.000059
39	1	0	3.261288	2.872920	-0.000030
40	1	0	-7.443851	0.274240	-0.884721
41	1	0	-7.519723	-1.282232	0.000230
42	1	0	-7.443883	0.274712	0.884401
43	1	0	7.519725	-1.282228	-0.000389
44	1	0	7.443867	0.274829	-0.884358
45	1	0	7.443865	0.274129	0.884764

Total Energy (HF) = 3697.1682725381 Hartrees

7. Polarizing optical microscopy (POM)

Polarizable optical microscopy images of *bay*-annulated PBIs on cooling from isotropic liquid state revealed the presence of macroscale crystalline domains due to their inherent structural anisotropic nature.

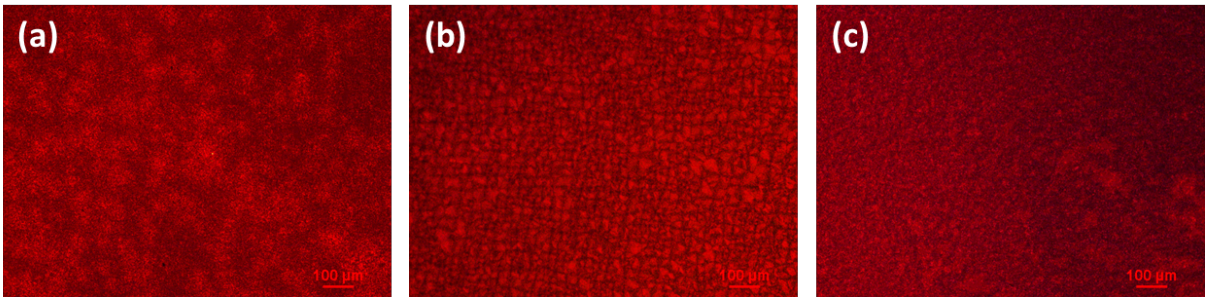

Figure S15. Polarizing optical microscopic images of (a) **PBI-N** at 114 ^{o}C, (b) **PBI-S** at 113 ^{o}C and **PBI-Se** at 135 ^{o}C.

8. Differential Scanning Calorimetry (DSC)

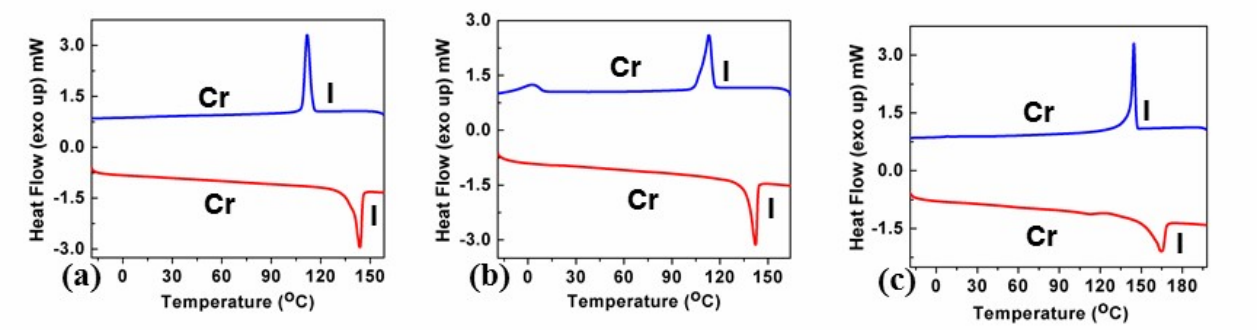

Figure S16. DSC scans of **PBI-N** (a); **PBI-S** (b) and **PBI-Se** (c) obtained for the second heating and first cooling scans at 5 ^{o}C/min under nitrogen atmosphere.

Table S1. Phase transition temperatures (^{o}C) and enthalpy changes (in kJ/mol)

S. No.	Compound	Heating	Cooling (in kJ/mol)
1	**PBI-N**	Cr 143.61 (21.77) I	I 111.75 (19.83) Cr
2	**PBI-S**	Cr 142.25 (19.16) I	I 112.90 (19.10) Cr
3	**PBI-Se**	Cr 164.46 (20.83) I	I 144.54 (19.86) Cr

9. Photophysical studies

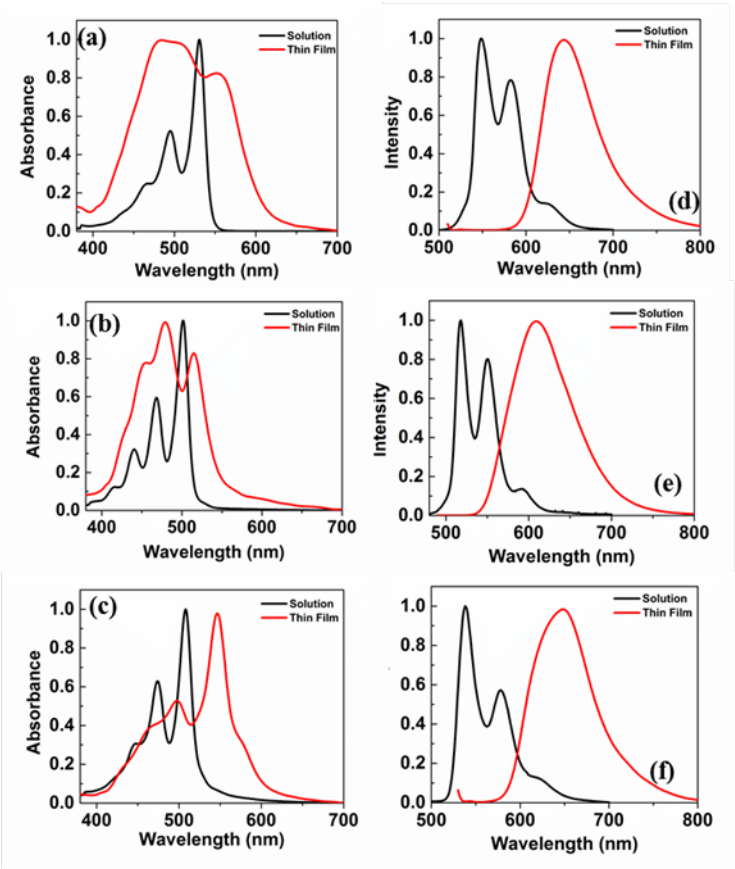

Figure S17. Normalized solution (black trace) and thin film (red trace) absorption spectra of **PBI-N** (a); **PBI-S** (b); **PBI-Se** (c); and normalized solution (black trace) and thin film (red trace) emission spectra of **PBI-N** (d); **PBI-S** (e); **PBI-Se** (f).

Table S2. Photophysical properties of *bay*-annulated PBIs.

	Solution[a]				Thin film[d]		
Compounds	Absorption (nm)	Emission[b] (nm)	Stokes shift (cm^{-1})	$\Delta E^{c}_{g,opt}$ (eV)	Absorption (nm)	Emission[e] (nm)	Stokes shift (cm^{-1})
PBI-N	531, 495, 467	549, 582	618	2.27	484, 552	643	5109
PBI-S	502, 468, 440	518, 551	615	2.40	456,479, 515	609	4457
PBI-Se	508, 474, 447	538, 578	1097	2.35	462, 498, 547	649	4672

[a]micromolar solutions in $CHCl_3$; [b]the excitation wavelength λ_{ex} = 531, 502 and 508 nm respectively for compounds **PBI-N, PBI-S and PBI-Se**; [c]calculated from the red edge of the absorption band; [d]spin coated in milimolar solution in toluene ; [e]the excitation wavelength λ_{ex} = 484, 479 and 498 nm respectively for compound **PBI-N**, **PBI-S** and **PBI-Se**.

10. Electrochemical properties

Table S3. Electrochemical[a,b] and thermal properties of *bay*-annulated PBIs.

Entry	E^{c}_{1red}	$E^{d,e}_{HOMO}$	$E^{d,f}_{LUMO}$	$\Delta E^{d,g}_{g,\ opt}$	T_c (°C)	T_d (°C)
PBI-N	-0.78	-5.74	-3.47	2.27	144	292
PBI-S	-0.67	-5.98	-3.58	2.40	142	264
PBI-Se	-0.66	-5.94	-3.59	2.35	164	285

[a]in Dichloromethane solutions; [b]Experimental conditions: $Ag/AgNO_3$ as reference electrode, Glassy carbon working electrode, Platinum wire counter electrode, TBAP (0.1 M) as a supporting electrolyte, room temperature; [c]in volts (V); [d]in eV; [e]Estimated from the formula $E_{HOMO} = [E_{LUMO} - \Delta E_{g(UV)}]$eV; [f]Estimated from the formula by using $E_{LUMO} = -[E_{red} - E_{1/2(Ferrocene)} + 4.8]$ eV; $E_{1/2\ (Ferrocene)} = 0.55$ eV,; [g]calculated from the red edge of the absorption band (548, 518, 528 nm respectively); T_c: clearing temperature by DSC; T_d: degradation temperature by TGA.

11. Atomic force microscopy (AFM)

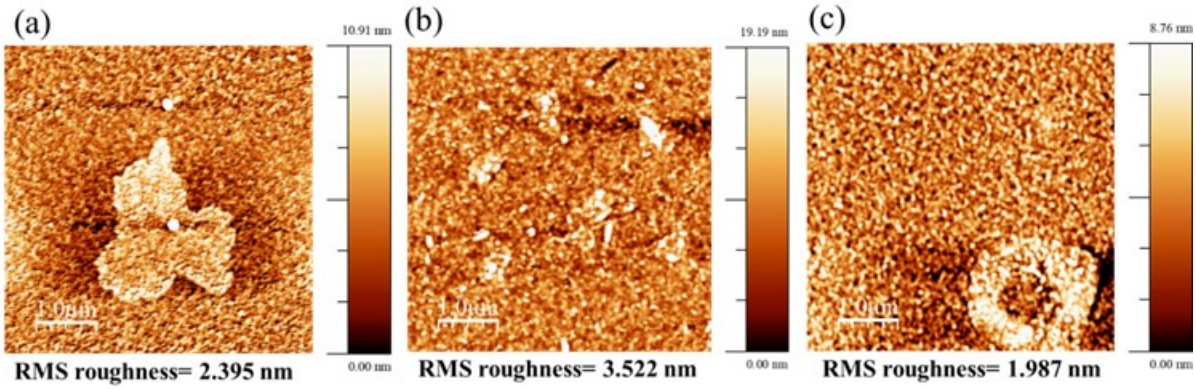

Figure S18. 5×5 AFM image of (a) **PBI-N**, (b) **PBI-S** and (c) **PBI-Se** on PMMA Surface.

The thin film morphology of the materials was characterized by AFM analysis. Higher surface roughness or irregularities in the active layer are determining factors that affect the device performance. Interfacial roughness leads to the formation of charge traps that hinder the charge conduction in the organic semiconductor materials. The images of the active layers were recorded by thermally depositing each of the materials on Al_2O_3/ PMMA coated-dielectric substrate at room temperature (~ 25 °C). It has been observed that the rms roughness of **PBI-N**, **PBI-S** and **PBI-Se** are 2.4 nm, 3.5 nm and 2.0 nm respectively (Figure S18), which is quite low and ideal for OFET fabrication.

12. Organic Field Effect Transistor (OFET) Characterization

OFETs based on **PBI-N, PBI-S** and **PBI-Se** molecules were fabricated by using Al_2O_3/PMMA-dual dielectric systems with a top-contact bottom-gate configuration. Figure 7 in the manuscript represented the typical schematic of the fabricated geometry of the devices. For the fabrication of the devices, initially glass slides were used as substrate onto which aluminum gate (~200 nm), was deposited by thermal evaporation method with the help of a shadow mask. The film was then subjected to anodization with a constant current density of 0.06 mA cm^{-2} at a voltage of 10 V, in the presence of 0.001 M citric acid monohydrate electrolyte solution at 20 °C. A square-shaped platinum mesh was used as a counter electrode to form ~13 nm Al_2O_3 layer over the Al film gate electrode. After iodization, to reduce the surface roughness, a 100 nm PMMA film was spin coated (obtained from a 30 mg/mL solution in anisole) and dried for 1 hour at 120 °C under nitrogen atmosphere. Following this, the active material [**PBI-N/PBI-S/PBI-Se**] was deposited by thermal deposition method (base pressure of 10^{-6} mbar). After that aluminum source-drain electrodes were thermally evaporated, at room temperature, up to a thickness of 80 nm to calculate three terminal properties of the materials. The fabricated OFETs were characterized by using a Keithley 4200 Semiconductor Characterization System in vacuum. The field-effect mobility in the saturation regime was extracted using equation,

$$I_{DS} = \frac{\mu_{sat} W C_i}{2L}\left(V_{GS} - V_{Th}\right)^2 \quad (1)$$

under the condition of $V_{DS} > (V_G - V_{Th})$, where I_{DS} is the source-drain current, μ is the field-effect mobility, W is the channel width, L is the channel length, C_i (= 25.83 $nF.cm^{-2}$) is the capacitance per unit area of gate dielectric layer, and V_{GS}, V_{Th} and V_{DS} are the gate, threshold and source-drain voltages respectively. Figure S18, S19 and S20 represent recorded output and transfer characteristics of **PBI-N, PBI-S** and **PBI-Se** molecules under vacuum condition. The details of all the device parameters are listed in Table S3

Table S4. Summary of device data.

Active Layer	[a]V_{Th} (V)	[b]W (μm)	[c]L (μm)	[d]Electron Mobility, μ ($cm^2/V.s$)	[e]I_{on}/I_{off}
PBI-N	6.17	800	40	3.87×10^{-3}	1.32×10^2
PBI-S	6.41	800	40	4.40×10^{-3}	3.98×10^2
PBI-Se	6.42	800	40	2.22×10^{-3}	3.73×10^2
[a]threshold voltage, [b]channel width, [c]channel length, [d]electron mobility and [e]current on to off ratio of the OFETs					

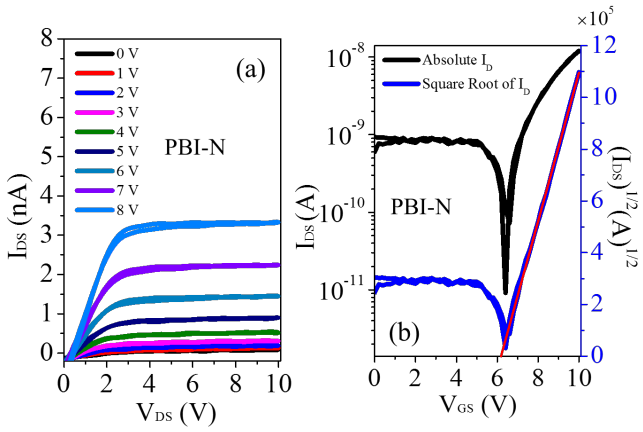

Figure S19. (a) I_D-V_D curves for **PBI-N** OFET for various values of V_G.(b) The I_D-V_G and $I^{1/2}$ vs. V_G curves for the same device for V_D=8 volts.

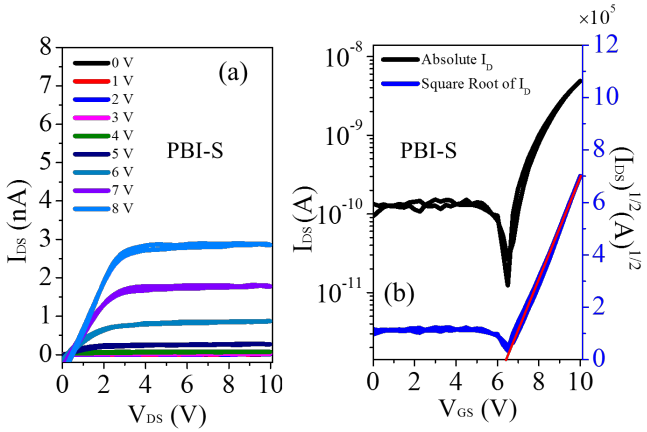

Figure S20. (a) I_D-V_D curves for **PBI-S** OFET for various values of V_G.(b) The I_D-V_G and $I^{1/2}$ vs. V_G curves for the same device for V_D=8 volts.

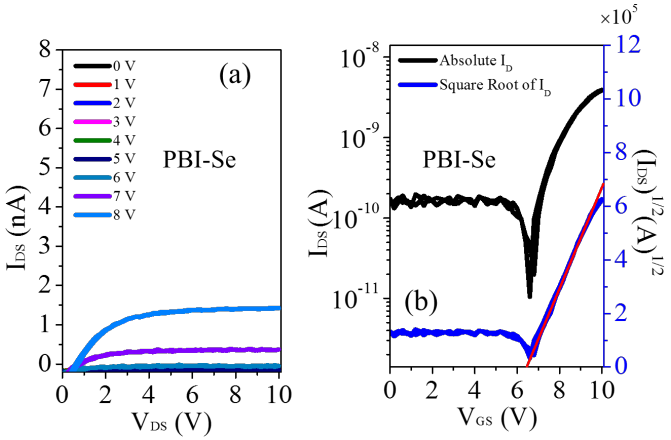

Figure S21. (a) I_D-V_D curves for **PBI-Se** OFET for various values of V_G. (b) The I_D-V_G and $I^{1/2}$ vs. V_G curves for the same device for V_D=8 volts

13. X-ray diffraction (XRD) studies

For the XRD analysis, thin film of the materials were prepared by thermal deposition method. Two sets of XRD data were recorded where in the first set were obtained for the films deposited on glass substrate whereas the second set were obtained for the films deposited on PMMA coated glass substrate. For the second set, initially, the PMMA was spin coated on the clean microscopic glass substrates at 3000 rpm for 60 seconds and dried at 110°C for 30 min. Followed by this, all the three materials are separately thermally deposited (~60 nm) on the substrate at 10^{-6} mbar of pressure. XRD studies were carried out with a Rigaku Micromax-007HF instrument with Cu Kα radiation (wavelength = 1.54184 Å). The calculated *d*-spacing for the respective peak positions are summarized in Tables below. To analyse the XRD pattern Scherrer formula $d = 0.9\lambda/\beta \cos\theta$ where used, where β is the full-width at half-maximum (FWHM) and λ is the wavelength of CuK_α radiation. It is evident that the sharp peaks observed in the small-angle regions support the packing of molecules in a layered (lamellar) crystalline packing.

Table S5. Summary of the XRD data obtained for the thin films on glass and PMMA coated glass substrates.

PBI-N				
2-theta(deg)	**Height(counts)**	**FWHM(deg)**	**d(ang.)**	**Size(ang.)**
3.006	16361.18	0.3588	29.36798	231.32
5.9706	315.93	0.4278	14.79059	194.21
9.0212	75.47	0.4256	9.79478	195.58
PBI-N with PMMA				
2-theta(deg)	**Height(counts)**	**FWHM(deg)**	**d(ang.)**	**Size(ang.)**
3.0188	17447.74	0.3205	29.24296	258.98
6.1575	223.96	2.1002	14.34228	39.56
8.9213	114.4	0.8627	9.90429	96.47
PBI-S				
2-theta(deg)	**Height(counts)**	**FWHM(deg)**	**d(ang.)**	**Size(ang.)**
3.4952	17474.95	0.3677	25.25847	225.74
6.9894	649.95	0.435	12.63691	191.11
10.3572	81.41	0.4836	8.53413	172.29
PBI-S with PMMA				
2-theta(deg)	**Height(counts)**	**FWHM(deg)**	**d(ang.)**	**Size(ang.)**
3.4736	13436.25	0.3853	25.41565	215.44
6.9622	513.83	0.4447	12.6861	186.94
10.4175	43.61	0.3542	8.48491	235.2
PBI-Se				
2-theta(deg)	**Height(counts)**	**FWHM(deg)**	**d(ang.)**	**Size(ang.)**
3.2546	5914.91	0.4662	27.12513	178.06
6.5437	134.31	0.6401	13.49661	129.83
PBI-Se with PMMA				
2-theta(deg)	**Height(counts)**	**FWHM(deg)**	**d(ang.)**	**Size(ang.)**
3.273	8323.22	0.4416	26.97224	187.95
6.5868	229.93	0.6155	13.40839	135.03

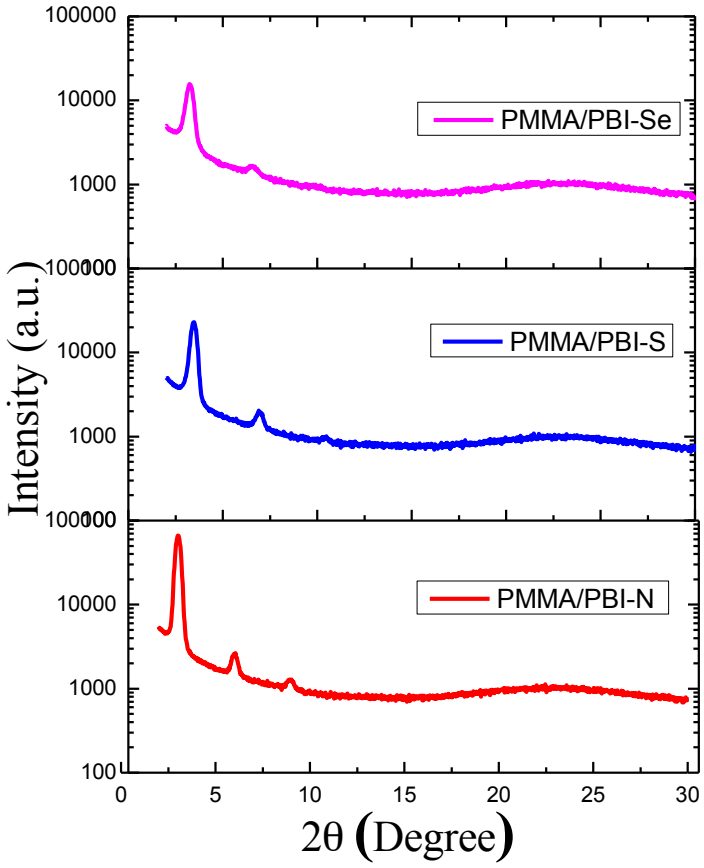

Figure S22. Intensity *vs* 2θ plots obtained for the thermally evaporated thin films of PBIs on PMMA coated glass substrates.

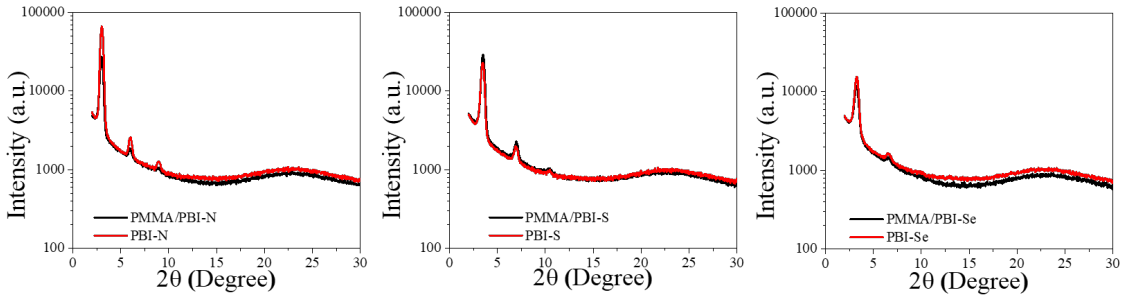

Figure S23. Overlap of Intensity *vs* 2θ plots obtained for the thermally evaporated thin films of PBIs on glass substrates and PMMA coated glass substrates.

14. References

1. Gupta, R. K.; Shankar Rao, D. S.; Prasad, S. K.; Achalkumar, A. S., Columnar Self-Assembly of Electron-Deficient Dendronized Bay-Annulated Perylene Bisimides. *Chem. Eur. J.* **2018,** *24*, 3566-3575.
2. Gaussian 09, Revision B.01, Frisch, M. J.; Trucks, G. W.; Schlegel, H. B.; Scuseria, G. E.; Robb, M. A.; Cheeseman, J. R.; Scalmani, G.; Barone, V.; Mennucci, B.; Petersson, G. A.; Nakatsuji, H.; Caricato, M.; Li, X.; Hratchian, H. P.; Izmaylov, A. F.; Bloino, J.; Zheng, G.; Sonnenberg, J. L.; Hada, M.; Ehara, M.; Toyota, K.; Fukuda, R.; Hasegawa, J.; Ishida, M.; Nakajima, T.; Honda, Y.; Kitao, O.; Nakai, H.; Vreven, T.; Montgomery, J. J. A.; Peralta, J. E.; Ogliaro, F.; Bearpark, M.; Heyd, J. J.; Brothers, E.; Kudin, K. N.; Staroverov, V. N.; Kobayashi, R.; Normand, J.; Raghavachari, K.; Rendell, A.; Burant, J. C.; Iyengar, S. S.; Tomasi, J.; Cossi, M.; Rega, N.; Millam, J. M.; Klene, M.; Knox, J. E.; Cross, J. B.; Bakken, V.; Adamo, C.; Jaramillo, J.; Gomperts, R.; Stratmann, R. E.; Yazyev, O.; Austin, A. J.; Cammi, R.; Pomelli, C.; Ochterski, J. W.; Martin, R. L.; Morokuma, K.; Zakrzewski, V. G.; Voth, G. A.; Salvador, P.; Dannenberg, J. J.; Dapprich, S.; Daniels, A. D.; Farkas, O.; Foresman, J. B.; Ortiz, J. V.; Cioslowski J.; Fox, D. J. Gaussian Inc., Wallingford, CT, **2009**.